Journal of Green Energy Research and Innovation

Performance Analysis of a Three-Level Z-Source Inverter for Grid-Connected Photovoltaic Systems Using Model Predictive Control

Ali Nahavandi, Mohammad Reza Azizi

Highlights

- **Presentation of a single-stage boost z-source neutral point clamped (Z-NPC) Inverter.**
- **Use of model predictive control (MPC) to control the proposed three-level inverter.**
- **Tracking the maximum point of power for photovoltaic panel (PV) using model predictive control.**

Graphical Abstract

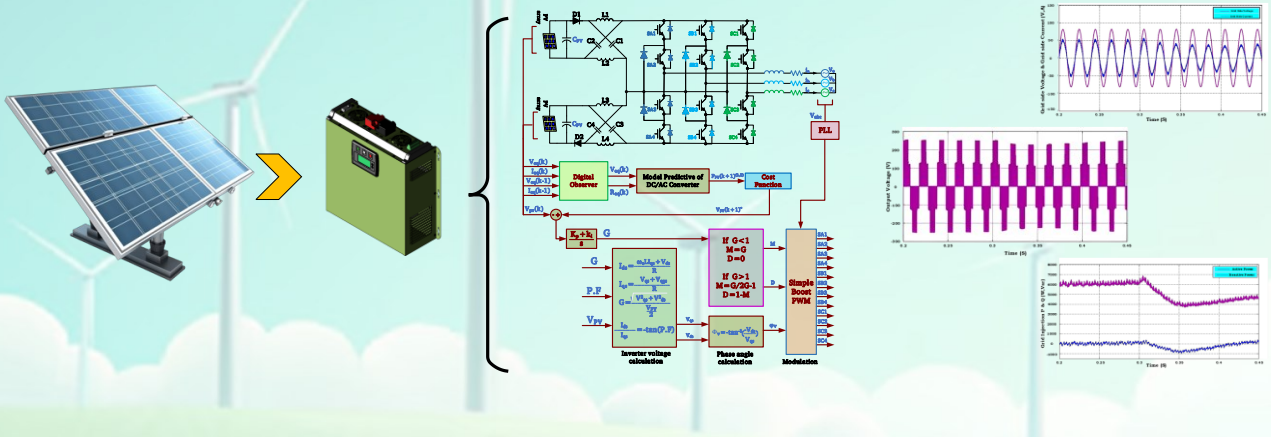

Use your device to scan and read the article online

Citation

A. Nahavandi, and M. Azizi," Performance Analysis of a Three-Level Z-Source Inverter for Grid-Connected Photovoltaic Systems Using Model Predictive Control," *Journal of Green Energy Research and Innovation*, vol. 2, no. 5, pp. 68-78, 2025.

https://doi.org/10.61186/jgeri.2.2.68

JGERI Journal of Green Energy Research and Innovation

Journal of Green Energy Research and Innovation 2.2 (2025) 68-78

Online ISSN: 3041-9018

Journal of Green Energy Research and Innovation

Journal Homepage: www.jgeri.araku.ac.ir

Performance Analysis of a Three-Level Z-Source Inverter for Grid-Connected Photovoltaic Systems Using Model Predictive Control

Ali Nahavandi *, Mohammad Reza Azizi

Department of Electrical Engineering, Faculty of Engineering, Malayer University, Malayer, Iran.

A R T I C L E I N F O

Keywords:
Photovoltaic System,
Three Level Z-Source Inverter,
Model Predictive Control,
Maximum Power Point Tracking
(MPPT).

Article History:
Received: 03 March 2025;
Revised: 07 April 2025;
Accepted: 09 April 2025.

Article type:
Research Article

* ***Corresponding author***
E-mail address
ali.nahavandi@malayeru.ac.ir (A. Nahavndi)

A B S T R A C T

In this paper, a single-stage three-level z-source inverter is utilized for connecting PV panels to the grid. The use of a three-level z-source inverter not only allows adjustment of output voltage but also facilitates the elimination of harmonic components. To extract maximum power from the PV panels, a model predictive control (MPC) strategy based on maximum power point tracking (MPPT) is employed. This method allows the MPC to predict the optimal operating point one step ahead, resulting in a faster response compared to conventional perturb and observe (P&O) method under rapid changes. Finally, the three-level z-source inverter is simulated using MATLAB/Simulink software, and its performance using the MPC method is analyzed. The simulation results have verified that the converter operates effectively.

1. Introduction

The increasing focus on renewable energy sources, driven by environmental concerns, decreasing prices of solar cells, and reductions in the costs of power electronic converters, has led to a significant rise in the use of solar panels for power supply and grid connectivity over the past decade [1]. The grid connection of solar panels is typically categorized into two forms: isolated and non-isolated. The non-isolated configuration is generally employed for low voltage applications, whereas the isolated configuration, which includes an iron core transformer, is used for high voltage applications. Although this transformer provides galvanic isolation between the power grid and photovoltaic systems, it is often bulky, heavy, and expensive due to its low operating frequency (50-60 Hz), leading to losses that diminish overall system efficiency. To eliminate the transformer, reduce costs, decrease weight, and enhance efficiency, there is a growing interest in transformerless systems [2,3].

Transformerless systems can be divided into single-stage and two-stage configurations. Grid-connected Photovoltaic (PV) systems typically employ two-stage architectures [4]. The first stage serves to boost the PV voltage and track the maximum power point using a DC-DC boost converter, while the second stage facilitates DC-AC power conversion. Although this two-stage structure has been tested successfully in recent years, it presents several disadvantages, including a high component count, lower efficiency, reduced functionality, increased costs, and bulkiness. To address these issues, there is growing interest in single-stage systems that can meet all requirements within a single power conversion stage. Several single-stage DC-AC inverters have been discussed in [5-7]. Among these single-stage systems, the impedance source inverter (ZSI) presents a particularly promising option for investigation. The ZSI possesses unique features that enable it to both increase and decrease the output voltage, capabilities that are not typically found in other types of inverters [8,9]. Generally, voltage source inverters (VSIs) can only decrease the output voltage, while current source inverters (CSIs) can only increase the output voltage. In [10] model predictive control was employed with a CSI to extract maximum power even when the PV voltage is less than its nominal value. One of the advantages of CSIs is their ability to deliver high-quality and robust current output.

However, a significant drawback of CSIs is the large DC link inductor, which can lead to high power losses. A ZSI with MPPT-based MPC was used in [11] to extract maximum power in a single stage, with satisfactory results.

PV arrays are inherently nonlinear, and they have a single operating point at which they generate maximum power. To maximize the efficiency of PV arrays, the implementation of Maximum Power Point Tracking control techniques is essential for extracting the maximum possible power [12]. Numerous MPPT techniques have been explored over the last couple of decades, with their respective advantages discussed in detail in [13]. Among these methods, the Perturb and Observe (P&O) technique is well-established and demonstrates satisfactory performance. However, its relatively slow response time can hinder its effectiveness in tracking rapid changes in solar irradiance [14,15]. A key contribution of this paper is the enhancement of the P&O method through the application of Model Predictive Control. By utilizing MPC, the P&O technique can predict the optimal operating point one step ahead compared to conventional P&O, allowing for a quick response to sudden changes in irradiance levels and temperature [16]. In [17], it was demonstrated that MPC can effectively improve the P&O method for MPPT, showing a strong response to rapid fluctuations in irradiance. Especially, this system is configured for grid connection using a two-stage approach, with each stage featuring independent control.

This paper focuses on a three-level impedance source inverter that employs MPPT-based MPC. This configuration not only facilitates the ability to increase or decrease output voltage and effectively implement MPPT but also reduces harmonic components in both the voltage and the current injected into the grid. Additionally, the inverter input is designed to incorporate two panels. Each panel is connected to its own impedance network, which enhances overall system performance. It is important to note that solar panels are typically constructed using low-voltage cells that are connected in series to achieve a reasonable output voltage. However, connecting a large number of cells in series can complicate the system and may negatively impact performance due to variations among cells and differing operating conditions. The subsequent sections of this paper are organized as follows: Section 2 describes the general components of the system. Section 3 presents the proposed MPPT-based MPC for z-source inverter. Section 4 provides simulation results that validate the effectiveness of the aforementioned control technique. Finally, Section 5 concludes the paper.

2. General Component of System

2.1. Three Level Z-Source Inverter

Three-level Neutral Point Clamped (NPC) inverters, known for their intrinsic advantages, are commonly employed as an effective architecture for medium voltage AC drives and, more recently, for grid-connected renewable energy applications at low voltage levels [18,19]. Despite their desirable output performance, these inverters have a limitation: they lack a DC-DC boost stage at the input, which restricts their functionality to only reducing the output voltage. To address this limitation, the NPC buck-boost impedance source inverter has been introduced [20,21]. This configuration incorporates two X-shaped impedance networks connected to two independent DC sources. The term "three-level Z-NPC" refers to this type of inverter. In a three-level Z-NPC inverter, instead of using two voltage sources or two capacitors with a common connection point, two Z-source inverters are employed without a common point. As a result, z-source inverters can operate within the structure of multilevel inverters. The added impedance networks are responsible for balancing and boosting the voltage by allowing short circuits at any inverter phase (known as the shoot-through state) without causing damage to the semiconductor switches. This is achieved through the inductances of the z-source, which help prevent sudden increases in current. As shown in Figure 1, the three-level Z-NPC inverter consists of two impedance networks, each connected to its own independent DC source. These impedance networks have the capability to enhance the input DC voltage.

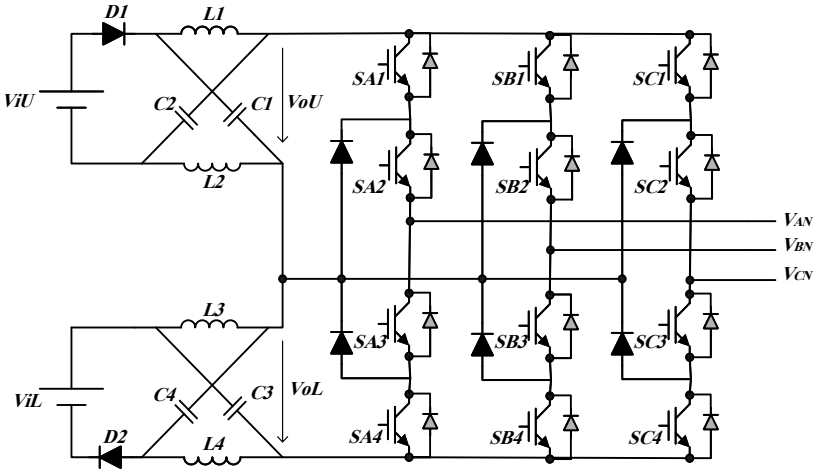

Figure 1. Three-level Z-source inverter with two impedance network.

Various modulation methods for z-source inverters have been proposed. Among these, in [22] the simple boost modulation strategy introduced which operates similarly to traditional carrier-based PWM, with its voltage gain defined by Equation (1):

$$G = M.B = \frac{V_{ac}}{V_o / 2} = \frac{M}{2M - 1} \tag{1}$$

Where M is the modulation index, B is the boosting factor of the impedance-network, V_{ac} is the amplitude of the output voltage of the inverter (equivalent to grid peak phase voltage when grid-tied), and V_o is the dc-link voltage. The boosting factor B is given by Equation (2):

$$B = \frac{1}{1 - 2D} \tag{2}$$

Where D is shoot-through duty cycle. Referring to the above equations, the boost factor of three level Z-NPC inverter for each impedance network can be derived as Equation (3):

$$\begin{cases} V_{oU} = B_U V_{iU} = \dfrac{V_{iU}}{1 - 2D_U} \\ V_{oL} = B_L V_{iL} = \dfrac{V_{iL}}{1 - 2D_L} \end{cases} \tag{3}$$

In which V_{iU} and V_{iL} are the DC input voltages and V_{oU} and V_{oL} are DC links output voltages and B_U and B_L for each impedance network are described as Equation (4):

$$\begin{cases} B_U = \dfrac{1}{1 - 2D_U} \\ B_L = \dfrac{1}{1 - 2D_L} \end{cases} \tag{4}$$

Where D_U is the shoot-through duty ratio for upper impedance network and for lower one is D_L as described in Equation (5):

$$\begin{cases} D_U = \dfrac{(T_{ShU} + T_{ShB})}{T} \\ D_L = \dfrac{(T_{ShL} + T_{ShB})}{T} \end{cases} \tag{5}$$

In these equations T_{ShU}, T_{ShL} and T_{ShB} represent the time durations of the short-circuit condition for the upper impedance network, the lower impedance network, and for both networks operating simultaneously, respectively. To minimize the output total harmonic distortion (THD), the boost factor must be determined such that the output voltages of both DC links in the networks are equal. When the DC link voltages of the NPC inverter are balanced, the same output power can be extracted from both DC links.

2.2. MPPT Techniques

Solar power generation systems utilize photovoltaic panels to convert sunlight directly into electricity. Under specific environmental conditions, there exists only one maximum power point (MPP) due to the nonlinear relationship between current and voltage (I-V). This peak power point fluctuates with changes in solar irradiance and operating temperature. The primary objective of implementing MPPT system is to ensure that the array of photovoltaic panels operates at the MPP, regardless of variations in irradiance, partial shading, or temperature. These factors can significantly impact the system's ability to achieve optimal performance. In recent years, many techniques have been proposed for MPPT, including the incremental conductance (INC) method, the P&O method, and the hill climbing method [13,15,23,24].

2.3. Model Predictive Control (MPC)

Model Predictive Control is a relatively new control technique applied for the control of power electronic converters [25]. Model predictive control has been used in low-switching-frequency power electronics for high-power applications since the 1980s [26]. Since high switching frequencies for the MPC algorithm required long calculation time, widespread adoption was not feasible at that time. In the past decade, with the improvement of high-speed microprocessors, interest in the application of MPC in power electronics with high switching frequency has increased considerably [27].

This method utilizes a mathematical model of the controlled system to predict its behaviour at each sampling instant k for the subsequent instant (k + 1). To determine the optimal state of the power converter, a cost function is defined. This function typically includes several constraints and control conditions. It generally encompasses the differences between reference values and predicted values of the controlled variables. Additionally, various components of this function represent specific constraints, such as limitations on switching frequency and other nonlinearities.

3. Proposed MPPT-Based Model Predictive Control Method

Figure 2 illustrates a grid-connected three-level Z-NPC inverter that utilizes two photovoltaic arrays in its DC links. Additionally, the control block diagrams for the proposed Maximum Power Point Tracking based model predictive control and other considerations are presented in this figure. The following sections will describe these blocks in detail, step by step.

3.1. Maximum Power Point Tracking- Based Model Predictive Control

The maximum power point tracking based on model predictive control is accomplished in two stages. In the first stage, the predictive model of the system is developed, and by applying the discrete-time model of the control variables used for predictions in the state-space model, two adaptive voltage values for the photovoltaic panels are predicted for the next sampling time. In the second stage, the cost function of the MPPT-based model predictive control tracks the voltage that maximizes the power drawn from the PV cells.

In this paper, due to the utilization of two panels, several approaches are suggested for implementing control methods:

1. Predictive equations can be extracted for each panel and its associated network, with the average modulation index considered. In this case, each network's impedance can be tailored to its specific conditions, allowing for different shoot-through duty cycles.

2. Regard to same conditions, predictive equations for one panel and its network be extracted, and other parameters appropriately be considered.

3. Both panels, be considered as a single panel and then predictive equations be extracted.

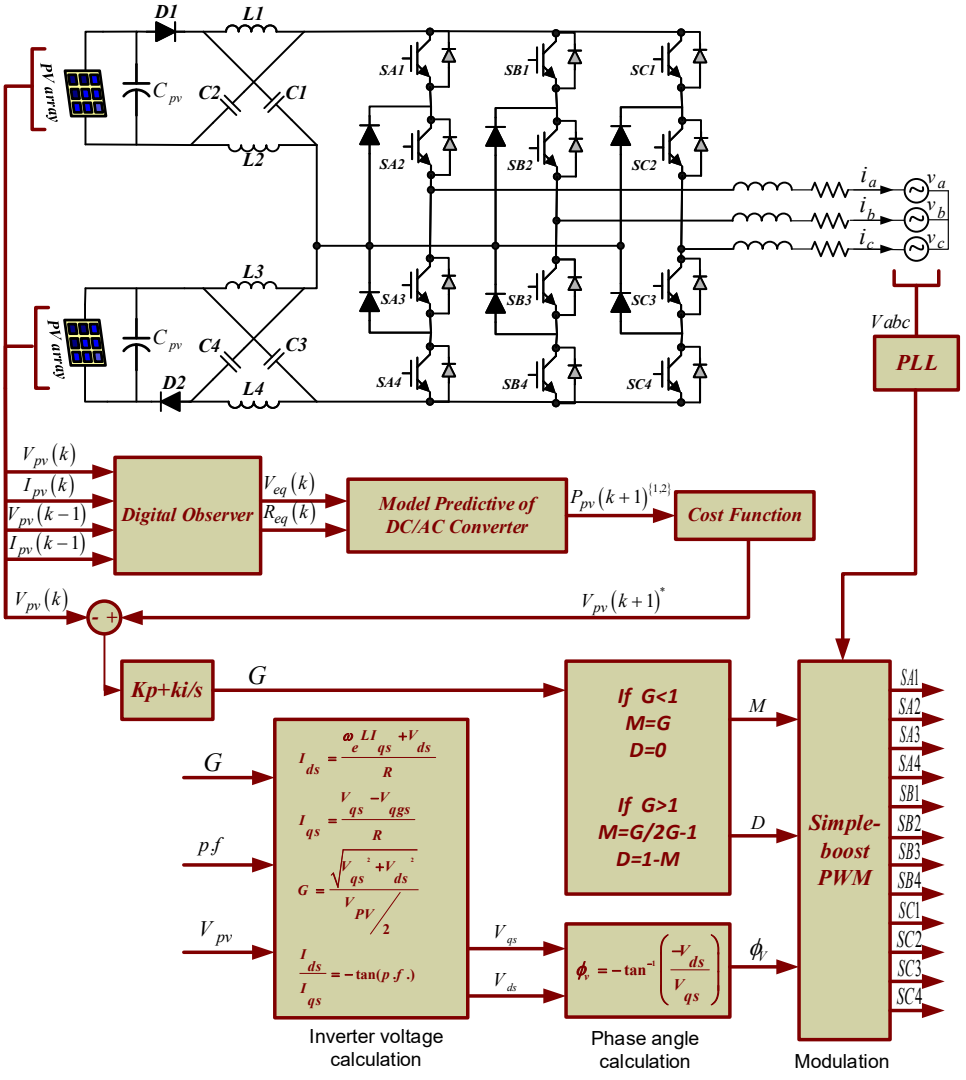

Figure 2. Three-level Z-source inverter with two impedance networks.

3.1.1. Stage1 Model Predictive Equation

By using KVL and KCL for non-shoot through state, Equation (6) is achieved.

$$\begin{cases} V_{PV} = R_{L_1} I_{L_1} + V_{L_1} + V_{C_1} \\ i_{L_1} = i_{C_1} + i_{inv} \end{cases} \tag{6}$$

Where R_{L1}, I_{L1} and V_{L1} are the inductor resistance, current and voltage respectively. Also, $V_{C1}$and i_{c1} are capacitor C_1 voltage and current respectively, and i_{inv} is inverter input current. By applying discrete time model with sample time T_s and replacing inductor voltage and capacitor current, this equation will be as Equation (7):

$$\begin{cases} I_{L_1}(k+1) = I_{L_1}(k) + \dfrac{T_s}{L_1}\left[(V_{PV} - V_{C_1}(k) - R_{L1} I_{L1}(K))\right] \\ V_{C_1}(k+1) = V_{C_1}(k) + \dfrac{T_s}{C_1}(I_{L_1}(k+1) - I_{inv}(k+1)) \end{cases} \tag{7}$$

Where I_{inv} is defined as Equation (8),

$$I_{inv}(k+1) = (S_{A1}.S_{A2}) \times I_a(k) + (S_{B1}.S_{B2}) \times I_b(k) + (S_{C1}.S_{C2}) \times I_c(k) \tag{8}$$

This equations for shoot through state are as Equation (9):

$$\begin{cases} V_{C2} = R_{L1} L_{L1} + V_{L1} \\ i_{L1} = -i_{C1} \end{cases} \tag{9}$$

As this topology is symmetrical and the values of inductance and capacitance is the same, $V_{L1} = V_{L2}$, $V_{C1} = V_{C2}$.

The discrete time model of above equation with sample time is as Equation (10):

$$\begin{cases} I_{L_1}(k+1) = I_{L_1}(k) + \dfrac{T_s}{L_1}(V_{C_1}(k) - R_{L_1} I_{L_1}(k)) \\ V_{C_1}(k+1) = V_{C_1}(k) - \dfrac{T_s}{C_1} I_{L_1}(k+1) \end{cases} \tag{10}$$

for sufficiently small sampling time (T_s), the change is negligible. Therefore, $V_{C_1}(k+1)$ is assumed to be approximately equal to $V_{C_1}(k)$. The average current flowing through C_{pv} and C_1 should be zero; thus, it can be concluded that I_{PV} is the same as Z-source inverter (ZSI) inductor current I_{L1}. Consequently, the predicted average PV current can be formulated using Equations (11) and (13) as follows:

$$I_{pv}^{ave}(k+1) = \left[I_{L_1}(k) + \frac{T_s}{L_1}(V_{PV} - V_{C_1}(k) - R_{L_1} I_{L_1}(k)) \right]\left[1 - D(k)\right] + \left[I_{L_1}(k) + \frac{T_s}{L_1}(V_{C_1}(k) - R_{L_1} I_{L_1}(k)) \right]\left[D(k)\right] \tag{11}$$

Considering the relationship between the PV voltage and V_{C_1} as follow in Equation (12):

$$V_{pv} = \frac{2}{B+1} V_{C_1} \tag{12}$$

The average PV voltage can be predicted using Equation (7), (10) and (12) as follows:

$$V_{pv}^{ave}(k+1) = \frac{2}{B+1} \times \left\{ \left[V_{C1}(k) + \frac{T_s}{C1}(I_{L1}(k+1) - I_{inv}(k+1)) \right]\left[1 - D(k)\right] + \left[V_{C1}(k) - \frac{T_S}{C1} I_{L1}(k+1) \right]\left[D(k)\right] \right\} \tag{13}$$

In following two possible values for PV voltage at sample time *(k+1)* will be predicted as follow in Equation (14):

$$\begin{cases} V_{pv}(k+1)^1 = V_{pv}(k) + \Delta V \\ V_{pv}(k+1)^2 = V_{pv}(k) - \Delta V \end{cases} \tag{14}$$

where ΔV is a voltage step that is adaptively predicted and can change based on its proximity to the Maximum Power Point (MPP). Equation (15) for ΔV is proposed:

$$\Delta V = \left| \tilde{V}_{pv}^{ave}(k+1) - V_{pv}(k) \right| \tag{15}$$

Where $V_{PV}^{ave}(k+1)$ is the predicted average voltage for PV at time n+1.

3.1.2. Stage2 MPPT Section & Cost Function

In this section, the MPPT technique tracks one of the two possible values of PV voltage that maximizes power extraction from the PV module. This MPPT algorithm requires understanding of the local P-V characteristics of the module around its operating point $V_{pv}(k)$. For this purpose, a digital observer (sensor) has been designed to generate the necessary information. The observer models the PV module with a Thevenin equivalent circuit. Since the characteristics of panel, at the time K and before it is available, Thevenin equivalent circuit of model can be achieved as shown in Figure 3. The elements of this circuit are equivalent voltage (V_{eq}) and equivalent resistance (R_{eq}) of the module and are calculated by Equation (16).

$$\begin{cases} R_{eq}(k) = -\dfrac{V_{pv}(k) - V_{pv}(k-1)}{I_{pv}(k) - I_{pv}(k-1)} \\ V_{eq}(k) = V_{pv}(k) + R_{eq}(k) \times I_{pv}(k) \end{cases} \tag{16}$$

Where $V_{pv}(k-1)$ and $I_{pv}(k-1)$ are the values of the PV module voltage and current from the previous sampling time. By calculating the panel voltage at the moment $k+1$ and having panel equivalent circuit, corresponding $I_{pv}(k+1)$ for each predicted value of voltage can be calculated in Equation (17):

$$\begin{cases} I_{pv}(k+1)^1 = \dfrac{V_{eq}(k) - V_{pv}(k+1)^1}{R_{eq}(k)} \\ I_{pv}(k+1)^2 = \dfrac{V_{eq}(k) - V_{pv}(k+1)^2}{R_{eq}(k)} \end{cases} \tag{17}$$

By estimating the equivalent resistance and voltage of the PV module and computing $I_{pv}(k+1)$ for each case, the two possible values for the generated power in the next sampling time can be easily predicted from Equation (18) and (19):

$$P_{pv}(k+1)^1 = V_{pv}(k+1)^1 \times I_{pv}(k+1)^1 \tag{18}$$

$$P_{pv}(k+1)^2 = V_{pv}(k+1)^2 \times I_{pv}(k+1)^2 \tag{19}$$

In next step, the predicted power value of the two cases will be used to evaluate the following cost function in Equation (20):

$$J^{\{1,2\}} = P_{pv}(k+1)^{\{1,2\}} - P_{pv}(k) \tag{20}$$

In order to track the MPP, the algorithm will choose the path that will result in the larger value of J from Equation (20). For instance, if $J_1 > J_2$, then the algorithm chooses to generate $P_{pv}(k+1)^1$ in the next sampling time, which correspondingly means the PV voltage will need to be shifted to $V_{pv}(k+1)^1$ by proper adjustment of controller. The desirable value of the PV voltage for the next step is denoted as $P_{pv}(k+1)^*$. Then $V_{pv}(k+1)^*$ will be compared with $V_{pv}(k)$ to generate the inverter gain.

3.2. Power Angle Control

The purpose of this section, is to control active and reactive power injected to the grid. To achieve such goal, inverter output voltages must be determined. The equivalent circuit of grid connected inverter in d-q rotating reference frame is shown in the Figure 4. Using the d axis and q-axis equivalent circuit, the relationship of d-q currents injected into the grid in terms of inverter output voltages is obtained as follow in Equations (21) and (22):

$$I_{ds} = \frac{\omega_e L I_{qs} + V_{ds}}{R} \tag{21}$$

$$I_{qs} = \frac{V_{qs} - V_{qgs}}{R} \tag{22}$$

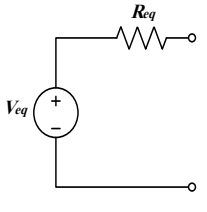

Figure 3. Equivalent circuit model of the PV module.

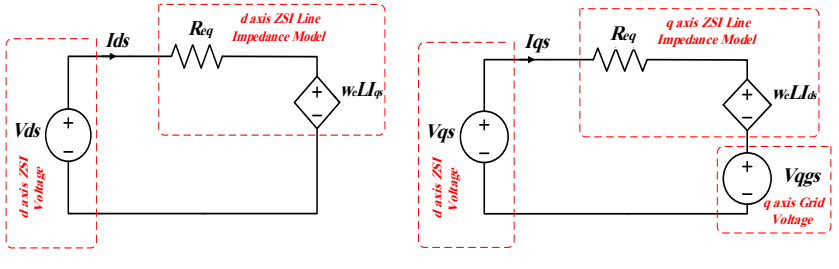

Figure 4. D-Q model of grid-connected Z-NPC system in rotating reference frame.

Where ω_e , L , R , V_{ds} , V_{qs} and V_{qgs} are grid angular frequency, line inductance, line resistance, inverter d-axis voltage, inverter *q*-axis voltage and the grid *q*-axis voltage, respectively.

According to Equation (1), the voltage gain of the inverter can be written as the follows in Equation (23):

$$G = \frac{V_{ac}}{V_{pv}/2} \tag{23}$$

In which we have V_{ac} as in Equation (24):

$$V_{ac} = \sqrt{V_{qs}^{\ 2} + V_{ds}^{\ 2}} \tag{24}$$

Also, there is Equation (25) for power factor:

$$\frac{I_{ds}}{I_{qs}} = -\tan(p.f) \tag{25}$$

Since unity power factor is concerned, by replacing 1 instead of $p.f$ in Equation (25), the *d*, *q* axis currents ratio will be obtained. By knowing inverter gain and solving these equations, the *d*, *q* axis voltages will be obtained. The power angle can be calculated using the following equation and be used in simple boost modulation as in Equation (26).

$$\phi_v = -\tan^{-1}\left(\frac{-V_{ds}}{V_{qs}}\right) \tag{26}$$

3.3. PI Controller & Calculation of M, D

In this section, the predicted voltage of the panel at a future time step is compared to the current panel voltage. The resulting error value is then fed into a PI controller to generate the inverter gain. This generated gain is subsequently utilized in the next block (Calculation of M and D) to determine the modulation index and duty cycle for the shoot-through state. The values of M, D determines how much the output voltage must be increased. In this block, the modulation index and duty ratio for the shoot-through state are defined according to the following equations:

For the case where the gain is less than or equal to unity we have Equation (27):

$$M = G,\ D = 0 \tag{27}$$

When the gain is greater than one we will have Equation (28):

$$M = G/2G - 1 \quad , \quad D = 1 - M \tag{28}$$

3.4. Switching of Three-Level Z-NPC Inverter

According to the three-level Neutral Point Clamped (NPC) inverter modulation based on the LS-PWM method, one of the three states presented in Table 1 is applied to the switches in the same leg at any given moment. A carrier wave with a frequency of 10 kHz and a range between (-1, 1) is compared with the values of positive and negative index modulation (-m, m), resulting in the generation of one pulse for each half-cycle. These pulses have been generated and added to conventional inverter pulses and create a shoot through state for Z-source inverter. If in mode 1 and 2 in the Table 1, the generated positive half-cycle pulses are applied to S_{A1} and S_{A3} at the same time, a shoot through state for upper impedance network will occur. Conversely, to achieve a shoot-through state in the lower impedance network, negative half-cycle pulses must be applied to the switches S_{A2} and S_{A4} , in the form of modes 2 and 3 in Table 1. It is important to note that in this method, there is no mode that allows both impedance networks to be in a shoot-through state simultaneously. In other words, there is no mode where all four switches in the same leg can be turned on at the same time.

Table 1. Switching table of three level NPC inverter.

Controller output	All switches in a leg			
	S_{A1}	S_{A2}	S_{A3}	S_{A4}
Mode 1	1	1	0	0
Mode 2	0	1	1	0
Mode 3	0	0	1	1

To achieve a shoot-through state in both impedance networks, the generated positive half-cycle pulses should be applied to S_{A1} and S_{A2} and the negative half-cycle pulses to S_{A3} add S_{A4}. According to the switching table, in modes 1 and 3, all four switches in a leg are turned on, resulting in both impedance networks being in a shoot-through state. It is important to note that this condition subjects the middle switches to increased voltage stress. Additionally, in mode 2 of the table, applying these pulses results in one of the two impedance networks entering a shoot-through state. Figure 5 illustrates the pulse generation for a leg of the inverter. In this figure, the black pulses correspond to the modulation of a three-level inverter, while the green pulses represent simple boost pulses. For clarity, the number of these pulses over a period (50 Hz) has been reduced.

As shown in Figure 5, in part A, it is indicated that simultaneously with the application of simple boost pulses to switches S_{A1} and S_{A2}, switch S_{A3} is also in inverter operation mode. The simultaneous turning on of these three switches causes the upper impedance network to be in shoot through state. In part B, with applying simple boost pulses to S_{A3} and S_{A4}, the switches S_{A1} and S_{A2} are switched in inverter operation mode. In this case, all four switches in a leg are turned on and both impedance network are in shoot through state. Similarly, in the specified part C, three lower switches are turned on. In this case, lower impedance network goes to shoot through state. Figure 6 illustrates the equivalent circuit for each of these states occurring in one leg of the inverter.

4. Simulation Results

In this section, the PV system is connected to the grid through a three-level Z-NPC converter. The effectiveness of the proposed MPC based MPPT strategy, along with other considerations discussed in the previous section, is evaluated using MATLAB/Simulink. The characteristics of SUNTECH270S-24-Vb module is used as an energy source of system. The P-V and I-V characteristic curves are illustrated in Figure 7, and the simulation parameters are summarized in Table 2. As mentioned in Section 3, a unity power factor is assumed for the system's operation. The performance of the MPC-based MPPT is assessed under three critical scenarios: response to a step change in solar irradiance, gradual changes in solar irradiance due to moving clouds, and steady-state performance around the maximum power point (MPP).

To begin evaluation, the operation of the system when the solar irradiance level decreases from 1000W/m^2 to 750W/m^2 at time t = 0.3 s is investigated. Figures 8 and 9 show the voltage and current of the upper PV panel connected to the three-level Z-NPC inverter, respectively. It is evident from these figures that the PV voltage and current at t = 0.3 s are affected by the change in irradiance level.

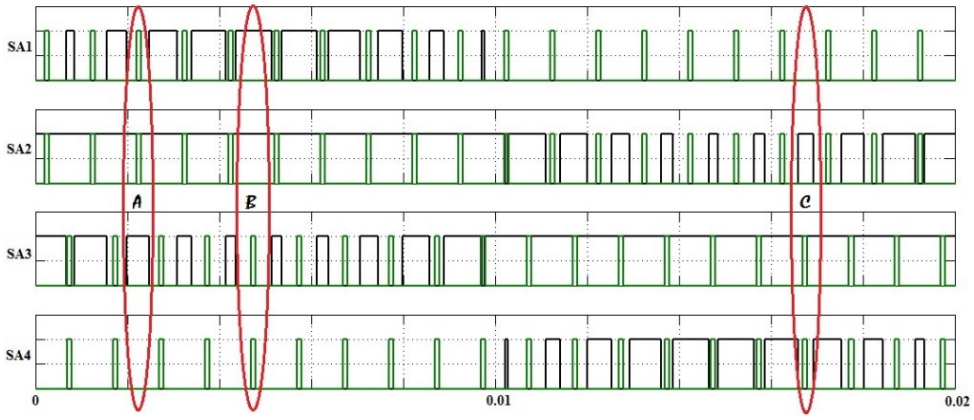

Figure 5. Modulation pulses for a leg of Z-NPC.

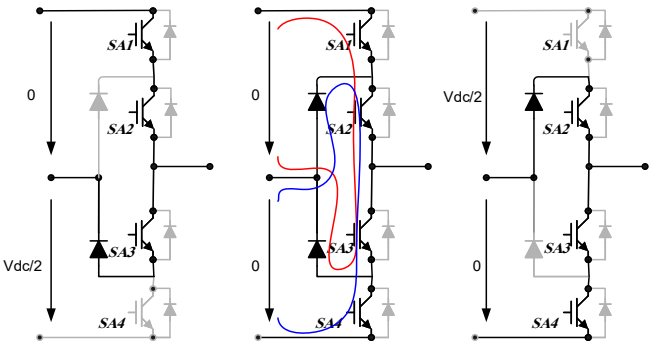

Figure 6. Shoot through states in a leg of Z-NPC.

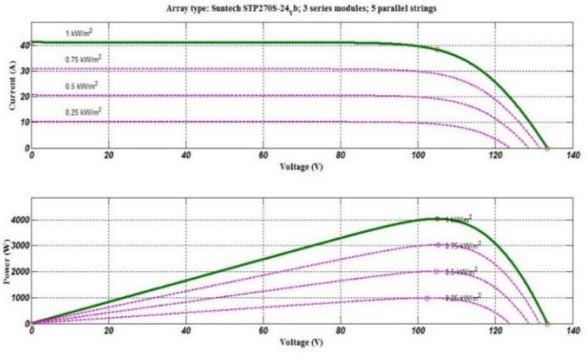

Figure 7. P–V and I–V characteristic curves of upper employed PV module.

Table 2. System parameters.

Parameters	Value
$L_1 = L_2 = L_3 = L_4 = L$	5 mH
$C_1 = C_2 = C_3 = C_4 = C$	1000 µF
C_{pv}	1000 µF
Sampling Time	5 µF
Switching frequency	10 kHz
L_{grid}	1 mH

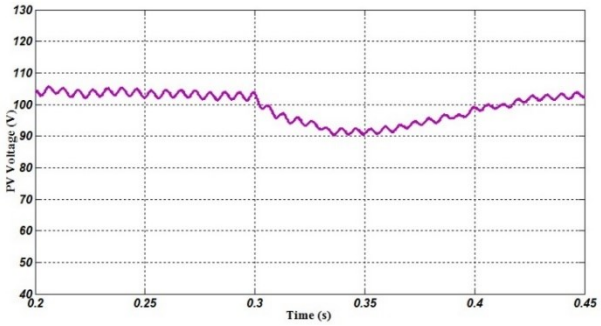

Figure 8. PV Panel Voltage for changing the irradiance level from 1000 W/m^2 to 750 W/m^2.

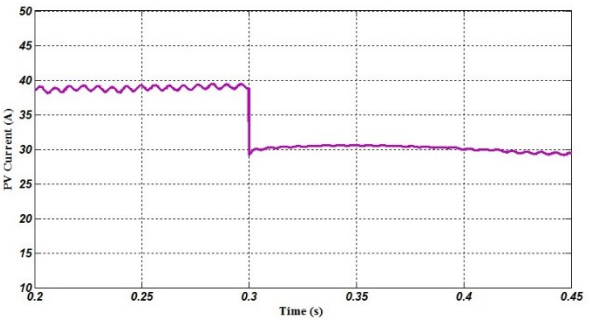

Figure 9. PV Panel current for changing the irradiance level from 1000 W/m^2 to 750 W/m^2.

The operating point of the PV system is optimized to extract maximum power. Figure 10 displays the output power of the upper panel, while the output power of the lower panel remains the same, as both impedance networks exhibit similar performance and operate at the same point. The overall power is obtained by sum of the power generated by each panel. As demonstrated, the proposed technique provides an acceptable response due to low convergence time and minimal oscillation around the maximum power point (MPP) in response to the applied step change in irradiance levels from 1000 to 750 W/m^2.

Figure 11 shows the unfiltered line output voltage of the inverter. The three-level waveform of the output voltage is clearly visible in this figure. At time t = 0.3 s, the output voltage is affected by a step change in irradiance. Subsequently, this voltage approaches the operating point value through the proposed control technique.

The generated power by the solar panels finally will be injected to grid through three-level Z-NPC inverter. It is important to note that during this transfer, some power is lost due to conduction and switching losses. Figure 12 shows the active and reactive power injected into the grid. As it's clear, the amount of power injected to grid, quickly decreases by applying step change in irradiance level. Also, with the aim of unity power factor that mentioned in previous part, it's visible that the reactive power is close to zero, means that the grid side voltage and current are in phase. Figure 13 shows the grid side voltage and current phase.

Figure 14 shows the harmonic components of the current injected into the grid using a three-level Z-NPC inverter. As can be seen from this figure, one of the advantages of the three-level Z-NPC inverter compared to the two-level Z-source inverter is its ability to reduce and eliminate high-order and even-order harmonics. Furthermore, the use of this inverter has led to decrease in the DC components of the grid-injected current. Table 3 compares the odd-order harmonic components of grid-injected current for both the two-level and three-level Z-source inverters. The table indicates that only the fifth and seventh harmonic components for the three-level inverter are greater than those for the two-level inverter, while all other odd harmonics in the two-level configuration have larger values.

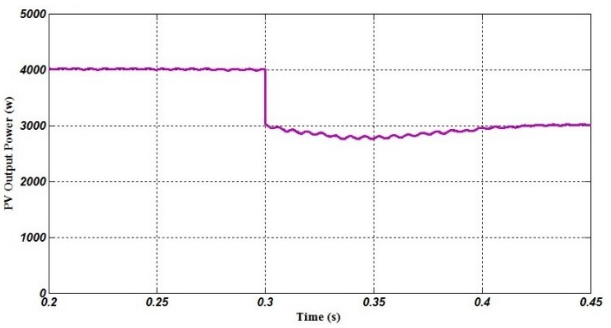

Figure 10. Extracted power from upper Solar Panel (extracted power from lower Panel is the same).

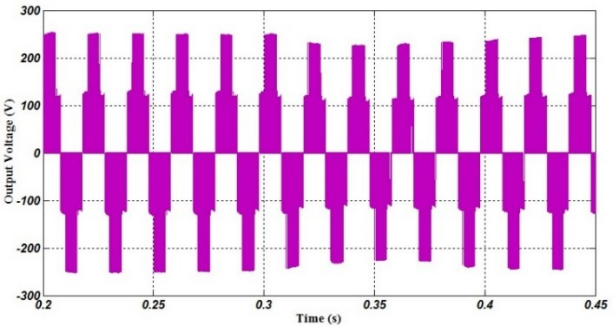

Figure 11. Line output voltage of three-level Z-NPC.

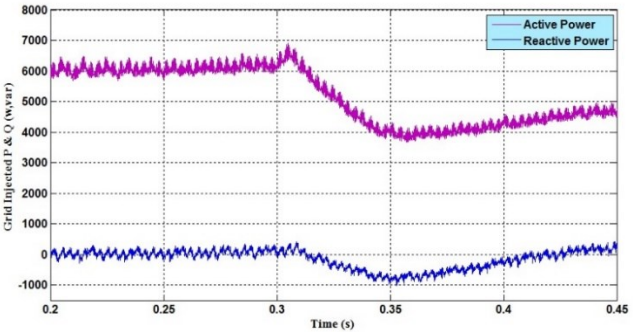

Figure 12. Injected Active and reactive power to grid.

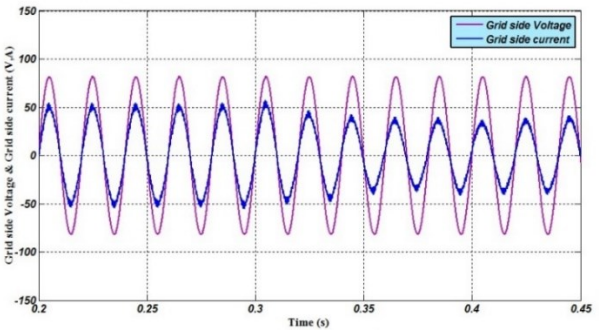

Figure 13. Grid side phase voltage and current.

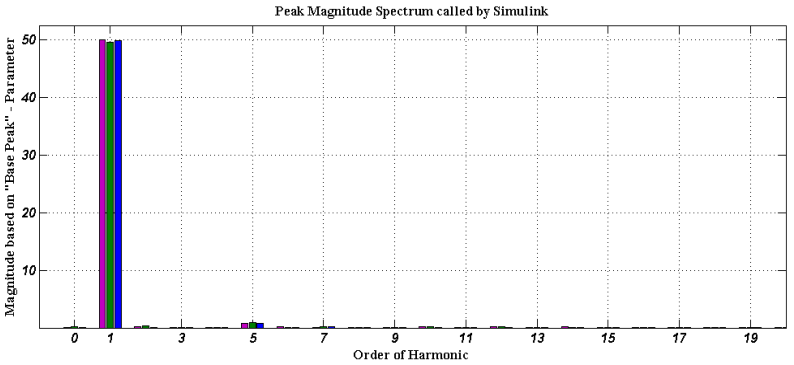

Figure 14. Spectrum of injected current to the grid.

Table 3. Comparison between the odd-order components of grid injected current for two-level and three-level Z-source inverter.

Harmonic order	Distortion in two-level inverter %	Distortion in three-level inverter %
Main component	48.91	49.95
3rd harmonic	0.7	0.1
5th harmonic	0.87	1.21
7th harmonic	0.67	0.24
9th harmonic	0.14	0.1
11th harmonic	0.51	0.02
13th harmonic	0.22	0.06
15th harmonic	0.06	0.08
17th harmonic	0.12	0.16
19th harmonic	0.12	0.04

5. Conclusion

In this paper, a model predictive control technique for maximum power point tracking in grid-connected PV panels was presented. The results showed that using the predictive control method, under step changes in solar irradiance, the maximum power point was tracked quickly with good convergence and minimal power ripple. Additionally, by incorporating both shoot-through and non-shoot-through states in the impedance source inverter, the PV panel was successfully connected to the grid while implementing MPPT. Using three-level Z-NPC inverter compared to the two-level Z-source inverter showed that the injected current in three-level mode, has fewer harmonic components. Furthermore, two panels were utilized, each with half the number of cells connected in series, which enhanced the performance capabilities of the PV system.

References

[1] P. Zhang, Y. Wang, W. Xiao, and W. Li, "Reliability Evaluation of Grid-Connected Photovoltaic Power Systems," *IEEE Transactions on Sustainable Energy*, vol. 3, no. 3, pp. 379–389, 2012.

[2] M. Shiravand, and A. Nahavandi, "Control and Improvement of Power Quality in Hybrid Three-Terminal AC/DC Microgrids," *Journal of Green Energy Research and Innovation*, vol. 1, no. 2, pp. 31–45, 2024.

[3] J. Ebrahimi, and M. Abasi, "Design of a Power Management Strategy in Smart Distribution Networks with Wind Turbines and EV Charging Stations to Reduce Loss, Improve Voltage Profile, and Increase Hosting Capacity of the Network," *Journal of Green Energy Research and Innovation*, vol. 1, no. 1, pp. 1–15, 2024.

[4] J. M. Kwon, B. H. Kwon, and K. H. Nam, "Three-Phase Photovoltaic System with Three-Level Boosting MPPT Control," *IEEE Transactions on Power Electronics*, vol. 23, no. 5, pp. 2319–2327, 2008.

[5] A. Nahavandi, M. Roostaee, and M. R. Azizi, "Single Stage DC-AC Boost Converter," *2016 7th Power Electronics and Drive Systems Technologies Conference (PEDSTC)*, pp. 362–366, 2016.

[6] S. Jain, and V. Agarwal, "A Single-Stage Grid Connected Inverter Topology for Solar PV Systems with Maximum Power Point Tracking," *IEEE Transactions on Power Electronics*, vol. 22, no. 5, pp. 1928–1940, 2007.

[7] E. Babaei, and A. Nahavandi, "Flexible Multilevel Boost DC-AC Converter," *2012 3rd Power Electronics and Drive Systems Technology (PEDSTC)*, pp. 506–511, 2012.

[8] F. Z. Peng, "Z-Source Inverter," *IEEE Transactions on Industry Applications*, vol. 39, no. 2, pp. 504–510, 2003.

[9] S. Patil, and P. Parikh, "Comparative Analysis of Simple Boost and Double Carrier PWM Control on PV Powered Z-Source Inverter," *2014 6th IEEE Power India International Conference (PIICON)*, pp. 1–6, 2014.

[10] B. Exposto, R. Rodrigues, et al., "Predictive Control of a Current-Source Inverter for Solar Photovoltaic Grid Interface," *2015 9th International Conference on Compatibility and Power Electronics (CPE)*, pp. 113–118, 2015.

[11] S. Sajadian, and R. Ahmadi, "Model Predictive-Based Maximum Power Point Tracking for Grid-Tied Photovoltaic Applications Using a Z-Source Inverter," *IEEE Transactions on Power Electronics*, vol. 31, no. 11, pp. 7611–7620, 2016.

[12] A. Bidram, A. Davoudi, and R. S. Balog, "Control and Circuit Techniques to Mitigate Partial Shading Effects in Photovoltaic Arrays," *IEEE Journal of Photovoltaics*, vol. 2, no. 4, pp. 532–546, 2012.

[13] T. Esram, and P. L. Chapman, "Comparison of Photovoltaic Array Maximum Power Point Tracking Techniques," *IEEE Transactions on Energy Conversion*, vol. 22, no. 2, pp. 439–449, 2007.

[14] H. Dong, H. Sugimoto, and N. Nishio, "A Maximum Power Tracking Control Method for Photovoltaic Power Generation System Based on Derivation of Output Power with Respect to Output Voltage," *IEEJ Transactions on Industry Applications*, vol. 118, no. 12, pp. 1435–1442, 1998.

[15] N. Femia, G. Petrone, G. Spagnuolo, and M. Vitelli, "Optimization of Perturb and Observe Maximum Power Point Tracking Method," *IEEE Transactions on Power Electronics*, vol. 20, no. 4, pp. 963–973, 2005.

[16] M. B. Shadmand, R. S. Balog, and H. Abu-Rub, "Model Predictive Control of PV Sources in a Smart DC Distribution System: Maximum Power Point Tracking and Droop Control," *IEEE Transactions on Energy Conversion*, vol. 29, no. 4, pp. 913–921, 2014.

[17] M. B. Shadmand, X. Li, R. S. Balog, and H. A. Rub, "Model Predictive Control of Grid-Tied Photovoltaic Systems: Maximum Power Point Tracking and Decoupled Power Control," *2015 First Workshop on Smart Grid and Renewable Energy (SGRE)*, pp. 1–6, 2015.

[18] Z. Tan, Y. Li, and M. Li, "A Direct Torque Control of Induction Motor Based on Three-Level NPC Inverter," *2001 IEEE 32nd Annual Power Electronics Specialists Conference (IEEE Cat. No.01CH37230)*, vol. 3, pp. 1435–1439, 2001.

[19] R. Strzelecki, "Three-Level Z-Source Neutral-Point-Clamped Inverter," *2006 8th International Conference on Actual Problems of Electronic Instrument Engineering*, pp. 172–179, 2006.

[20] P. D. Van den Heever, S. Oberholzer, and J. H. R. Enslin, "High-Efficient Solar Panel/Wind Turbine Converter with Maximal Power Control," in *Proceedings of the European Conference on Power Electronics and Applications*, pp. 663–668,1989.

[21] S. Alepuz, S. Busquets-Monge, et al., "Interfacing Renewable Energy Sources to the Utility Grid Using a Three-Level Inverter," *IEEE Transactions on Industrial Electronics*, vol. 53, no. 5, pp. 1504–1511, 2006.

[22] S. Dehghan, E. Seifi, M. Mohamadian, and R. Gharehkhani, "Grid Connected DG Systems Based on Z-Source NPC Inverters," *2011 2nd Power Electronics, Drive Systems and Technologies Conference*, pp. 104–110, 2011.

[23] P. C. Loh, D. Vilathgamuwa, Y. S. Lai, G. T. Chua, and Y. Li, "Pulse-Width Modulation of Z-Source Inverters," in *Conference Record of the 2004 IEEE Industry Applications Conference, 39th IAS Annual Meeting*, vol. 1, pp. 148–155, 2004.

[24] A. F. Boehringer, "Self-Adapting Dc Converter for Solar Spacecraft Power Supply Selbstanpassender Gleichstromwandler Für Die Energieversorgung Eines Sonnensatelliten," *IEEE Transactions on Aerospace and Electronic Systems*, vol. AES-4, no. 1, pp. 102–111, 1968.

[25] J. Rodriguez, and P. "Cortes, Predictive Control of Power Converters and Electrical Drives," *John Wiley & Sons*, 2012.

[26] J. Holtz, "A Predictive Controller for The Stator Current Vector of AC Machines Fed from A Switched Voltage Source," in *Proceedings of the International Power Electronics Conference (IPEC-Tokyo)*, pp. 1665–1675, 1983.

[27] J. Rodriguez, M. P. Kazmierkowski, et al., "State of the Art of Finite Control Set Model Predictive Control in Power Electronics," *IEEE Transactions on Industrial Informatics*, vol. 9, no. 2, pp. 1003–1016, 2013.

Declaration of competing interest

The authors declare that they have no known competing financial interests or personal relationships that could have appeared to influence the work reported in this paper. The ethical issues, including plagiarism, informed consent, misconduct, data fabrication and/or falsification, double publication and/or submission, redundancy, have been completely observed by the authors.

Bibliography

Ali Nahavandi was born in Malayer, Iran, in 1983. He received the B.Sc., M.Sc. and Ph.D. degrees in electrical power engineering from University of Tabriz, Tabriz, Iran, in 2006, 2008 and 2014 respectively. Since 2014 he is assistant professor in Faculty of Engineering, Malayer University, Malayer, Iran. His research interests include power electronic converters, renewable energy systems and power quality.

Email: ali.nahavandi@malayeru.ac.ir

ORCID: 0000-0002-8036-188X

Contribution Statement: Conceptualization, Project administration, Supervision, Validation, Roles/Writing - original draft, Writing-review & editing.

Mohammadreza Azizi received the B.Sc. degree in electrical engineering from the Shahid Madani University of Azerbaijan, Tabriz, Iran, and the M.Sc. degree in electrical engineering from Malayer University, Malayer, Iran. He acquired several years of experience as a Lecturer and a Research Assistant at Malayer University.

Email: Azizi.malayeru@gmail.com

ORCID: 0000-0002-5599-2276

Contribution Statement: Conceptualization, Data curation, Formal analysis, Investigation, Resources, Software.